II. Using small mirrors to construct piecewise linear mirror surfaces for solar cookers

E.R. Vrscay

First version of this manuscript: June 23, 2024
Latest version: October 25, 2025

Introduction

Our first generation of real solar cookers will be constructed from 4" $\times$ 4" mirrors. As in our previous study, we first consider cookers which are obtained by translating the graphs of convex functions such as $y = f(x) = x^2$ along the z-axis to produce parabolic-like troughs.

In this case, however, the functions $f(x)$ are approximated by piecewise linear functions in order to take into consideration the flatness of the mirrors which comprise the cooker.

Case No. 1: $f(x) = x^2$

We must first produce a piecewise linear approximation to $f(x) = x^2$ with linear pieces of (mirror) length $b = \frac{1}{3}$ (feet). For simplicity, we choose the approximation to be the **interpolation** of $f(x) = x^2$ so that the endpoints (x_n, y_n) of the linear "pieces" satisfy the condition $y_n = f(x_n) = x_n^2$. The FORTRAN program `linterp.f` was written to produce such an approximation. (Details on the method used to compute these endpoints will be given in Appendix 1.) Numerically, we observe that five linear pieces are required to produce an approximation to $f(x) = x^2$ over the interval $[0, 1]$. The endpoints (x_n, y_n) of these five mirrors of length $\frac{1}{3}$ are presented below.

n	x(n)	y(n)
0	0.0000000000	0.0000000000
1	0.3176872874	0.1009252126
2	0.5673059903	0.3218360866
3	0.7671940331	0.5885866845
4	0.9359675009	0.8760351628
5	1.0838643199	1.1747618640

Plots of $f(x) = x^2$ and its linear interpolation to the end of the fifth linear piece are shown in Figure 0 below.

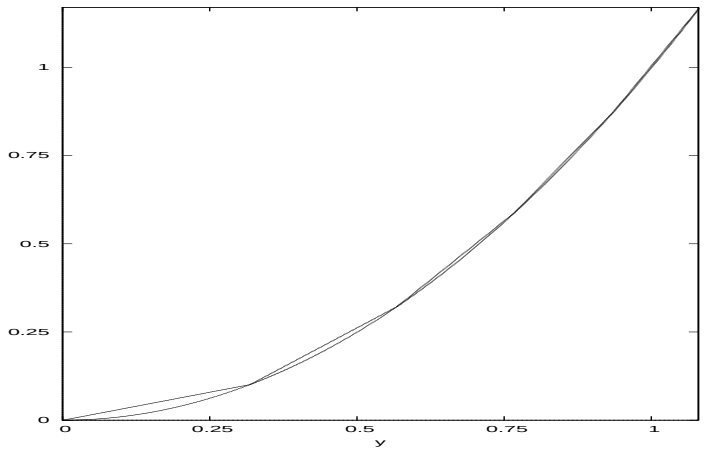

Figure 0: Plot of $f(x) = x^2$ and its linear approximation with the first five "pieces" of length $b = \frac{1}{3}$.

The FORTRAN program `raylinterp.f` was written in order to compute the y-intercepts of rays parallel to the y-axis travelling from $y = \infty$ and reflected by the linear "pieces". (The program `raylinterp.f` was a modification of the program `raydist4.f` from Study I which used the functional form of the linear "pieces". Details will be provided in an appendix.) The results obtained from the use of the endpoints tabulated above are shown in Figure 1 below in the form of a histogram distribution. (Note that as in Study I, only rays that were reflected directly onto the non-negative y-axis were employed in the histogram. Rays that would theoretically be reflected into this region after more than one encounter with a mirror were not counted.) Note that the bulk of the distribution appears to be concentrated over the range $y \in [0.1, 0.4]$.

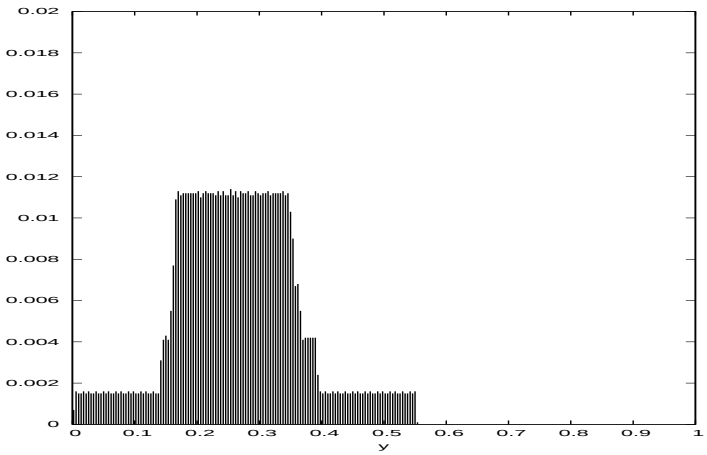

Figure 1: Distribution of first-reflected rays from piecewise linear interpolation of $y = f(x) = x^2$ with pieces of length $b = \frac{1}{3}$.

We also mention that the program `raydist4.f` was checked by computing the reflections produced by individual mirrors. In each case, the parallel rays hitting an individual mirror were reflected onto an interval of the y-axis. As the slope of the mirror increased (i.e., linear pieces that lay farther away from the y-axis, the length of this interval decreased.

As another check, the piecewise linear approximation of $y = f(x) = x^2$ using 15 linear pieces of length $b = 0.1$ (to produce an approximation over $[0, 1]$) was computed using program `linterp.f`. The endpoints of this approximation were then used used in program `raylinterp.f` to produce the distribution of reflected rays shown in Figure 2 below. As expected, this distribution is more peaked, i.e., less diffuse, than the previous one and therefore "closer" to the Dirac delta function situated at $y = \frac{1}{4}$ which corresponds to the single focal point of the parabola $y = x^2$.

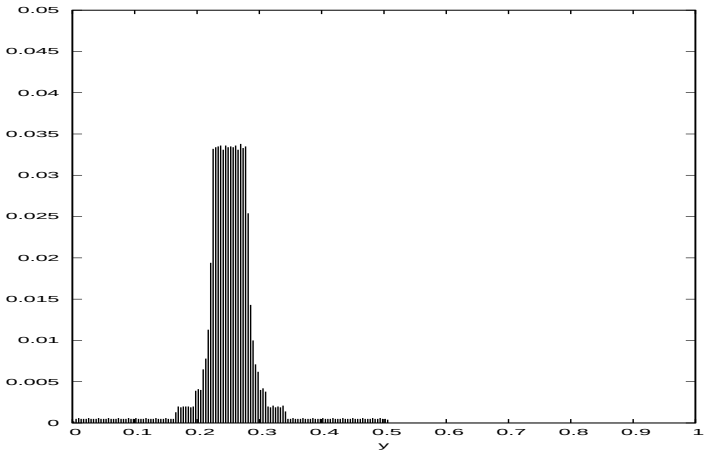

Figure 2: Distribution of first-reflected rays from piecewise linear interpolation of $y = f(x) = x^2$ with 15 pieces of length $b = 0.1$.

Case No. 2: $y = f(x) = \frac{1}{2}x^2$

We now investigate briefly the shallower trough produced by the function $f(x) = \frac{1}{2}x^2$. The endpoints of the first five pieces of length $b = \frac{1}{3}$ are presented below.

0	0.0000000000	0.0000000000
1	0.3289150449	0.0540925534
2	0.6295147384	0.1981444030
3	0.8946367885	0.4001874917
4	1.1289531226	0.6372675766
5	1.3388297995	0.8962326160

The distribution of reflected rays along the y-axis is shown in Figure 3 below. A comparison with Figure 1 shows that, as perhaps expected since the parabolic trough is now shallower, the distribution of reflected rays is spread over a wider range. Moreover, the bulk of the distribution in Figure 3 is concentrated over the range of values $y \in [0.3, 0.7]$ as opposed to the range $[0.15, 0.4]$ in Figure 1.

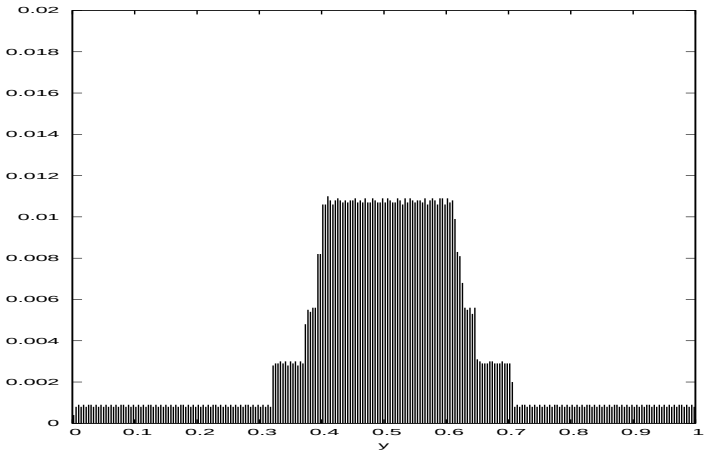

Figure 3: Distribution of reflected rays from piecewise linear interpolation of $y = f(x) = \frac{1}{2}x^2$ with pieces of length $b = \frac{1}{3}$.

Solar Cooker No. 1: Parabolic trough with cross-sectional formula $y = f(x) = x^2$

At this preliminary stage, as mentioned earlier, we are using 4" $\times$ 4" mirrors to construct our cookers. The first such cooker, a parabolic trough employing the convex function $y = f(x) = x^2$ (x, y in feet) is shown in Figure 4 below.

Figure 4: "Solar Cooker No. 1: Parabolic trough with cross-sectional formula $y = f(x) = x^2$ employing 4" $\times$ 4" mirrors.

One slight modification had to be made to the computations presented earlier since, as can be seen above, the mirrors are spaced 0.25" apart in order to allow bending of the cardboard on which they are mounted. As such, the parameter b representing the lengths of the components of the piecewise linear interpolation functions must be adjusted to 4.25". The coordinates of the first six endpoints (in feet) of the linear pieces are given below:

0	0.0000000000	0.0000000000
1	0.3357479939	0.1127267154
2	0.5949977699	0.3540223462
3	0.8012215555	0.6419559810
4	0.9749732576	0.9505728531
5	1.1271178903	1.2703947387

Since the cooker was constructed using inches/feet, the above values were converted to inches,

0	0.0000000000	0.0000000000
1	4.0289759268	1.3527205849
2	7.1399732387	4.2482681541
3	9.6146586657	7.7034717715
4	11.6996790916	11.4068742373
5	13.5254146841	15.2447368646

These are the positions at which the nails at side of the cooker, shown in Figure 5 below, are located. These nails provide the connection between the side panel and the piecewise linear trough on which the mirrors are attached.

Figure 5: Photo of one of the sides of Solar Cooker No. 1 showing the positions of the nails which attach the side of the cooker to the trough. The nails are located at the endpoints of the mirrors, the linear "pieces" which interpolate the cross-sectional formula $y = f(x) = x^2$.

Solar Cooker No. 2: 2D cooker composed of four parabolic troughs with cross-sectional formula $y = f(x) = x^2$.

We then considered a very simple two-dimensional cooker which is composed of four semi-parabolic troughs. Each of these troughs is composed of 9 4" $\times$ 4"-inch mirrors and the bottoms of the troughs are connected to a square base as shown in Figure 6 below.

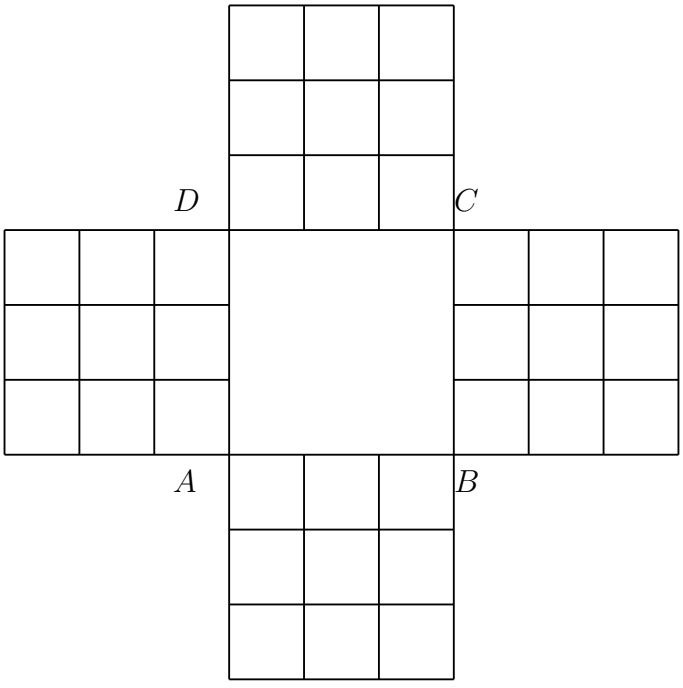

Figure 6: Configuration of two-dimensional Solar Cooker No. 2 composed of four parabolic troughs.

The square base $ABCD$ may also be filled with 9 mirrors which can reflect light upwards into the central portion of the cooker.

Upon further reflection (no pun intended), however, we decided that this configuration might be too "rectangular" or "square" and that each of the 3×3-mirror components was too wide. Moreover, we thought that it might not be possible to install many mirrors in the triangular regions between these components. (The overall shape of the cooker would be octagonal.) This led to the next cooker configuration.

Solar Cooker No. 3: 2D cooker composed of 8 parabolic troughs with cross-sectional formula $y = f(x) = x^2$.

As is seen in Figure 7 below, it was decided to take one of the three radial rows of mirrors of each component and rotate it with respect to the center. This produced four semi-parabolic troughs which were two mirrors wide along with four semi-parabolic troughs only one mirror wide. It was thought that the latter set of troughs would focus more light into the middle of the cooker.

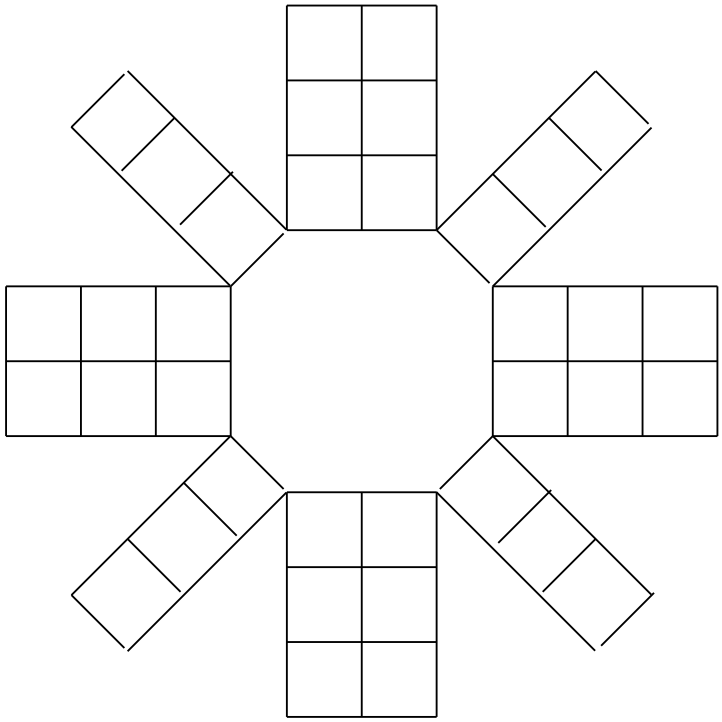

Figure 7: Configuration of two-dimensional Solar Cooker No. 3 composed of four major and four minor semi-parabolic troughs.

There are some options for the regions between the radial troughs. We decided to cut wedge-like pieces that would connect continuous troughs, keeping their parabolic form. (Note that these pieces are "wedge-like", as opposed to purely triangular.) These pieces were covered with aluminum foil. The result is shown in Figure 8 below.

It was then decided to attach one mirror at the upper portion of each of these pieces covered with aluminum foil. Some mirrors were also attached in the central octagonal region, but this is still in an experimental stage. (The mirrors are slanted toward the center, as opposed to lying on the flat octagonal base.) The result is shown in Figure 9 below.

Figure 8: Solar Cooker No. 3, almost final version.

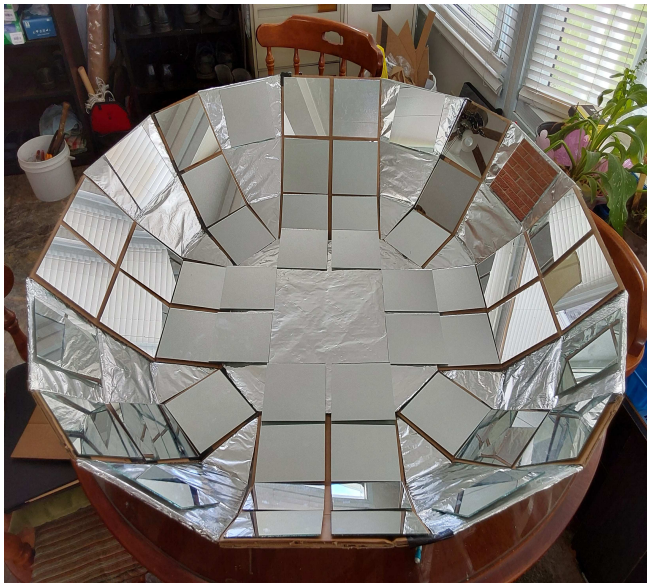

Figure 9: Solar Cooker No. 3, final version.

Appendix 1. A Newton-Raphson method to compute endpoints to piecewise linear approximations of functions

We consider the piecewise linear approximation of a function $f(x)$ with pieces of length $b > 0$. In our solar-cooker applications, $f(x)$ is usually even so we'll consider, for simplicity and without loss of generality, only non-negative values of x. The situation is sketched in the figure below.

The linear approximations, or simply "pieces", are supported on intervals $I_n = [x_{n-1}, x_n]$, $n \geq 1$, where $x_0 = 0$, with the conditions,

$$(x_{n+1} - x_n)^2 + [f(x_{n+1}) - f(x_n)]^2 = b^2 \quad n = 0, 1, 2, \cdots . \tag{1}$$

Starting with x_0, approximations to the interpolation points x_n, $n \geq 1$, of desired accuracy can be computed recursively, i.e., from x_0 we compute x_1, from which we compute x_2, etc..

Our Newton-Raphson-like method is as follows. Given x_n, $n \geq 0$, we wish to find x such that

$$h(x) = (x - x_n)^2 + [f(x) - f(x_n)]^2 - b^2 = 0 \, . \tag{2}$$

(For simplicity of notation, we omit any reference to n in the notation for h.) For our Newton-Raphson function, we need to compute $h'(x)$,

$$h'(x) = 2(x - x_n) + 2[f(x) - f(x_n)]^2 f'(x) \, . \tag{3}$$

Our Newton-Raphson (NR) function is then given by

$$N(x) = x - \frac{h'(x)}{h(x)} \, . \tag{4}$$

In practice, if we know x_n, we can let $x = x_n + \epsilon$ be the starting point for the NR method where $\epsilon > 0$ is "reasonable", not too large, not too small, e.g., $b/2$?

In the computation presented in Table 1, the approximations x_n were determined to an accuracy well beyond 10^{-10}. Numerically, the lengths of the five "pieces" obtained from these x_n, i.e.,

$$l_n = \sqrt{(x_n - x_{n-1})^2 + (f(x_n) - f(-x_{n-1}))^2} \qquad 1 \leq n \leq 5 \, , \tag{5}$$

approximate $b = \dfrac{1}{3}$ to at least 10 decimal digits, i.e., 0.3333333333.

Appendix 2. Determining the y-intercepts of rays reflected from the piecewise linear approximations to a mirror function $f(x)$ as well as the density distributions of these rays.

With reference to Appendix 1, we consider the piecewise linear interpolation of $f(x)$ supported on the interval $I_n = [x_{n-1}, x_n]$, $n \geq 1$, as sketched below. The endpoints of this "piece" are (x_{n-1}, y_{n-1}) and (x_n, y_n), where

$$y_{n-1} = f(x_{n-1}) \qquad y_n = f(x_n)\,. \tag{6}$$

If we let $y = g_n(x)$ be the (affine) function defining this linear "piece", then a point $(x, g_n(x))$ on this line is given by

$$\frac{g_n(x) - y_{n-1}}{x - x_{n-1}} = \frac{y_n - y_{n-1}}{x_n - x_{n-1}} = m_n\,, \qquad x_{n-1} \leq x \leq x_n\,, \tag{7}$$

where m_n is the slope of the "piece" with support I_n. A rearrangement of Eq. (7) yields

$$g_n(x) = y_{n-1} + m_n(x - x_{n-1}) \qquad x_{n-1} \leq x \leq x_n\,. \tag{8}$$

We'll now use the following result of our previous paper: Suppose that a ray travelling downward and parallel to the y-axis along the line $x = a > 0$ is reflected from the mirror surface $y = f(x)$ at the point $(a, f(a))$ toward the y-axis. Then the y-intercept of the reflected ray is

$$d(a) = f(a) - \frac{a}{2}f'(a) + \frac{a}{2f'(a)}\,. \tag{9}$$

We now consider any ray which travels downward and is reflected by the linear "piece" supported on $I_n = [x_n, x_{n-1}]$. The equation of this "piece" is given by $g_n(x)$ in Eq. (8) so we replace $f(x)$ with $g_n(x)$ to give

$$d(a) = g_n(a) - \frac{a}{2}g_n'(a) + \frac{a}{2g_n'(a)}\,. \tag{10}$$

From Eq. (8),

$$g_n'(x) = m_n = \frac{y_n - y_{n-1}}{x_n - x_{n-1}}\,, \qquad x_{n-1} \leq x \leq x_n\,, \tag{11}$$

and we obtain the following result for $d(a)$,

$$d(a) = y_{n-1} + \frac{y_n - y_{n-1}}{x_n - x_{n-1}}(a - x_{n-1}) - \left(\frac{a}{2}\right)\frac{y_n - y_{n-1}}{x_n - x_{n-1}} + \left(\frac{a}{2}\right)\frac{x_n - x_{n-1}}{y_n - y_{n-1}}\,, \qquad x_{n-1} \leq a \leq x_n\,. \tag{12}$$

Note that d is an affine function of a which implies that interval $I_n = [x_{n-1}, x_n]$ (incoming rays) is transformed to an interval $J_n = [d_n, e_n]$ on the y-axis (reflected rays) by means of a (linear) scaling followed by a translation. Let us now determine d_n and e_n.

Some important remarks: Note that we have designated the interval J_n as $[d_n, e_n]$ and **not** $[d_n, d_{n+1}]$. The reason for this is that it is not guaranteed – in fact, it would be a rather special case – that the contiguous intervals J_n and J_{n+1} on the y-axis share a common endpoint, as is the case for the I_n on the x-axis. Without getting into any formulas right now (that will come later), we simply state that the right endpoint e_n of J_n will depend upon the right endpoint (x_n, y_n) of the linear "piece" supported on I_n as well as the slope m_n of this "piece". The left endpoint d_{n+1} of interval J_{n+1} will depend upon the left endpoint (x_n, y_n) of the linear "piece" supported on I_{n+1} – the same point used for the computation of e_n – as well as, however, the slope m_{n+1} of this linear "piece". As such, it is not guaranteed that $e_n = d_{n+1}$. In other words, two different linear "pieces" are being used to generate these two endpoints.

At this point, the reader may wonder, "So which "piece" actually reflects the light ray that impinges upon a **boundary point** of the interval I_n?" The answer is, "It doesn't matter. Boundary points are isolated points and therefore negligible with respect to the continuum of the real numbers. (They are also negligible

with respect to the physical reality that is being modelled!) It is the interior points of the intervals I_n which contribute to any "accumulation" of reflected rays. The set of all interior points of I_n, namely, the open interval (x_{n-1}, x_n) is reflected into the interior open interval of J_n, namely, (d_n, e_n). A proper and rigorous treatment of this problem would take care of these technicalities. Here, we shall work with closed intervals and assume that the complications arising from boundary points can be addressed.

That being said, it is quite possible that the intervals J_n of reflected rays can overlap with each other at more than isolated boundary points. Some examples presented below will demonstrate this. In fact, the behaviour is even more striking than may have been first imagined.

Returning to our main discussion, we now determine d_n and e_n, the endpoints of J_n. Setting $a = x_{n-1}$ in Eq. (12),

$$d_n = d(x_{n-1}) = y_{n-1} + \left(\frac{x_{n-1}}{2}\right)\left[-m_n + \frac{1}{m_n}\right]. \tag{13}$$

Setting $a = x_n$ in Eq. (12),

$$e_n = d(x_n) = y_n + \left(\frac{x_n}{2}\right)\left[-m_n + \frac{1}{m_n}\right]. \tag{14}$$

We now assume that the mirror function $f(x)$ is increasing for $x > 0$, implying that $m_n > 0$, and use Eqs. (13) and (14) to compute $\|J_n\|$, the length of the interval J_n as follows,

$$\|J_n\| = e_n - d_n = y_{n+1} - y_n + \frac{1}{2}(x_{n+1} - x_n)\left[-m_n + \frac{1}{m_n}\right]. \tag{15}$$

In the special case, $m_n = 1$, the term in square brackets on the right side of Eq. (15) vanishes so that

$$e_n - d_n = y_{n-1} - y_n = x_n - x_{n-1} \quad \Longrightarrow \quad \|J_n\| = \|I_n\|. \tag{16}$$

This is to be expected since the linear mirror "piece" lies at an angle of $\frac{\pi}{4}$ with respect to the x-axis. As a result, the incoming vertical rays are reflected to become horizontal rays which travel leftward. Let us now see if we can determine the change in length in general. We'll rewrite Eq. (15) as follows,

$$\begin{aligned}
\|J_n\| &= e_n - d_n \\
&= (x_n - x_{n-1})\left(\frac{y_n - y_{n-1}}{x_n - x_{n-1}}\right) + \frac{1}{2}(x_n - x_{n-1})\left[-m_n + \frac{1}{m_n}\right] \\
&= (x_n - x_{n-1})\left[m_n - \frac{1}{2}m_n + \frac{1}{2}m_n\right] \\
&= \frac{1}{2}\left[m_n + \frac{1}{m_n}\right]\|I_n\|,
\end{aligned} \tag{17}$$

where $\|I_n\|$ denotes the length of interval I_n. The remarkable result is that for any $m_n > 0$ but $m_n \neq 1$, the term in square brackets is **greater than two**. It might be easy to see this graphically, but let's provide a "proof".

$$h(x) = x + \frac{1}{x}. \tag{18}$$

Clearly $h(1) = 2$. Moreover, for any $x > 0$,

$$h(x) = h\left(\frac{1}{x}\right). \tag{19}$$

Let's now assume that

$$x + \frac{1}{x} > 2 \quad \forall\ x > 0 \ \text{ except } \ x = 1. \tag{20}$$

and see if we arrive at a contradiction. Multiply both sides by $x > 0$ and rearrange to give

$$x^2 + 1 > 2x \quad \Longrightarrow \quad x^2 - 2x + 1 > 0 \quad \Longrightarrow (x-1)^2 > 0. \tag{21}$$

Clearly, the above is true for all $x > 0$ except $x = 1$. This leads to the remarkable conclusion based on Eq. (17):

Given a linear mirror "piece" with support I_n and with slope $m_n > 0$ but $m_n \neq 1$. Then the length of the interval J_n (obtained from a reflection of interval I_n) is longer than the length of interval I_n.

Only in the case $m_n = 1$ is the length of J_n equal to that of I_n.

An interesting side note: At this point, the reader may be asking: "Hey, wait a minute! If the angle of incidence equals the angle of reflection, the widths of the incoming and reflected beams for a given linear mirror "piece" should be the same! What goes on here?"

The reader is entirely correct that the widths of incoming and reflected beams are equal. The length of the interval J_n of reflected rays on the y-axis, however, is **not**, in general, width of the beam since the beam is generally striking the y-axis at an angle to the normal of the y-axis. Only in the special case of a 45^o mirror, where the reflected beam travels horizontally, does the length of J_n coincide with the width of the beam.

This suggests that the coefficient multiplying the term $\|I_n\|$ in Eq. (17) is, in some way, related to the angle – perhaps its cosine? – between the beam and the normal to the y-axis, i.e., the x-axis. Let us examine a sketch of the situation shown in Figure 10. Here we show a linear mirror "piece" supported over the interval

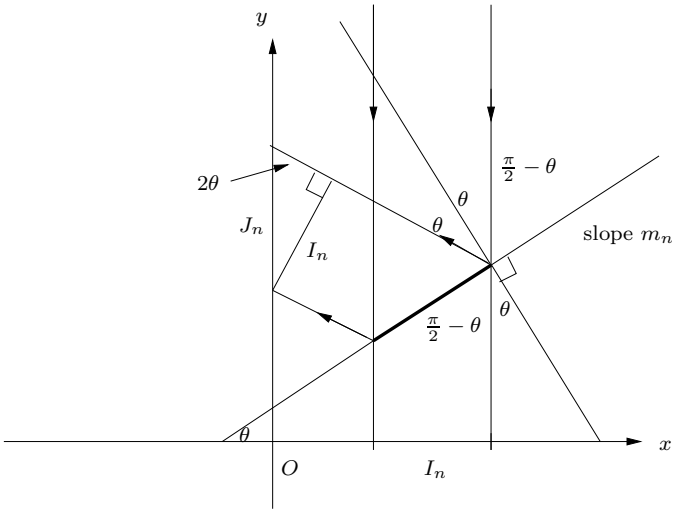

Figure 10

I_n. A downward moving vertical beam of rays with width $\|I_n\|$. The reflected beam of width $\|I_n\|$ then strikes the y-axis to produce interval J_n. A number of relevant angles have been identified in the figure. Note that the angle between the reflected beam and the y-axis is $2\theta_n$ where θ_n is the angle of incidence of the incoming beam with respect to the normal of the linear "piece". This implies that

$$\|J_n\| \sin 2\theta_n = \|I_n\| \quad \Longrightarrow \quad \|J_n\| = \frac{\|I_n\|}{\sin 2\theta_n} \,. \tag{22}$$

We've found our trigonometric relationship between $\|J_n\|$ and $\|I_n\|$. The next step is to see if we can rewrite the $\sin 2\theta_n$ term in the denominator in terms of m_n, the slope of the linear "piece." (The answer appears to have been given in Eq. (17) but we should really derive it.) But just before proceeding, let's perform a quick check of the above result to see that we are on the right track. When $\theta_n = \dfrac{\pi}{2}$, Eq. (22) implies that $\|J_n\| = \|I_n\|$, which we know to be true from our previous discussions. Things are looking good.

From Figure 10, it follows that the line on which the linear "piece" lies has orientation angle θ_n with respect to the x-axis. This implies that

$$m_n = \tan\theta_n = \frac{\sin\theta_n}{\cos\theta_n} \,. \tag{23}$$

By using an appropriate right triangle with side lengths 1 and m_n and therefore a hypotenuse of length $\sqrt{1+m_n^2}$

(Exercise) we see that

$$\sin\theta_n = \frac{m_n}{\sqrt{1+m_n^2}}\,, \qquad \cos\theta_n = \frac{1}{\sqrt{1+m_n^2}}\,. \tag{24}$$

Let us now return to the coefficient on the right side of Eq. (17),

$$\begin{aligned} \frac{1}{2}\left[m_n + \frac{1}{m_n}\right] &= \frac{m_n^2+1}{2m_n} \\ &= \frac{1}{2\sin\theta_n\cos\theta_n} \\ &= \frac{1}{\sin 2\theta_n}\,. \end{aligned} \tag{25}$$

Therefore, Eq. (17) becomes

$$\|J_n\| = \frac{1}{\sin 2\theta_n}\,\|I_n\|\,, \quad 0<\theta<\frac{\pi}{2}\,, \tag{26}$$

in agreement with Eq. (22). where θ_n is the angle of orientation of the linear "piece" with respect to the x-axis. Once again, note that only in the case $\theta_n = \dfrac{\pi}{4}$ are the lengths of the two intervals equal.

Obtaining estimates of the distribution of rays hitting a mirror composed of linear "pieces"

Returning to Eq. (17), we see that for all $m_n > 0$ except $m_n = 1$, there is an **expansion** of the width of the incoming interval of rays I_{n+1} after reflection. At first glance, this might seem incorrect. We can certainly see that in the case $m_n = 1$, i.e., a straight mirror inclined at $\dfrac{\pi}{4}$ to the x-axis, the width of the interval remains the same. In the case $m_n \neq 1$, one may be tempted to think that the reflected rays also travel horizontally. Using such reasoning, simple geometry would show that in the case $m_n < 1$, the interval I_{n+1} is **compressed** and in the case $m_n > 1$, the interval I_{n+1} is **expanded**. Such reasoning is incorrect, however, **since the reflected rays are no longer travelling in parallel, nor are they travelling horizontally!** In the case $m_n < 1$, the reflected rays are travelling **leftward and upward.** In the case $m_n > 1$, the reflected rays are travelling bf leftward and downward. From Eq. (17) there is a symmetry between m_n and $1/m_n$, i.e., you get the same result if $m_n = A$ or $m_n = 1/A$ for some $A > 0$. In both cases, you get a spreading of the originally parallel rays.

Now consider a mirrored surface composed of several piecewise linear components, e.g., piecewise linear interpolation of $f(x) = x^2$ as shown in Figure 0. Now imagine a "homogeneous" beam of light rays travelling downward and parallel to the y-axis. (By "homogeneous", we mean that the rays have equal intensity at all $x = a \geq 0$.) From our discussion above, the set of light rays which hits a given "piece" which is supported on an interval $I_n = [x_{n-1}, x_n]$, i.e., light rays situated at $a \in I_n$ will be reflected to the interval $J_n = [d_{n-1}, d_n]$ on the y-axis, where d_n is given in Eq. (13).

Let us now suppose that we model the beam of light rays which impinge on the mirror by means of a discrete and uniformly distributed set of parallel, downward travelling rays situated at locations $x_n = a_n = n\Delta a$ where Δa is very small. For simplicity of discussion, define Δa as follows,

$$\Delta a = \frac{1}{N}\,, \tag{27}$$

where N a very large integer, e.g., 100 or 1000. This implies that there are roughly N rays in each unit interval $[n, n+1]$ on the (positive) x-axis. The number of rays, r_n, hitting the nth "piece" supported on interval I_n, $n \geq 1$, is therefore directly proportional to the length of I_n. In fact, we may assume, with an error of only about one or two, that

$$r_n = \text{int}\,[N(x_n - x_{n-1})]\,, \qquad n \geq 1\,, \tag{28}$$

where "int" denotes "integer part of". (We could also allow for non-integer values of rays in which case the "int" would not be needed.)

This implies that r_n rays will be reflected onto the interval $J_n = [d_{n-1}, d_n]$ with length $d_n - d_{n-1}$. Since the transformation mapping interval I_n to J_n is affine, the distribution of the r_n rays over J_n will be uniform. Recall that only in the case that the slope of the linear mirror "piece" $m_n = 1$ is the length of J_n equal to that of I_n. In all other cases where $m_n > 0$, the length of J_n is greater than that of I_n. In these latter cases, the r_n rays will be farther apart from each other on J_n than they were on I_n. The spacing between these rays over J_n will be (with near zero error)

$$\Delta b_n = \frac{\|J_n\|}{\|I_n\|}\,\Delta a = \left[\frac{1}{\sin 2\theta_n}\right]\,\Delta a\,, \qquad n \geq 1\,, \tag{29}$$

where we have used Eq. (26), with θ_n being the angle of orientation of the linear mirror "piece" with respect to the x-axis.

A greater spacing Δb_n between rays over an interval J_n compared to their spacing Δa_n over the interval I_n can be interpreted as a lessening of the **density of rays** – which measures the **intensity** of the beam – on J_n as compared to that of I_n. The distribution of rays on J_n, however, is still uniform, as it was over I_n.

On this note, the (one-dimensional or "lineal") **density** of rays, often denoted as "$\rho(x)$", can be defined in this discrete case as the number of rays per unit length. From our definition of the spacing of rays Δ in Eq. (27), the lineal density of our incoming rays is given by

$$\rho(x) = \rho_0 = N = \frac{1}{\Delta a}\,. \tag{30}$$

Note that we have added a subscript "0" to the Greek letter "ρ". This is a quite standard manner to denote the constancy of a parameter such as density in a problem being studied.
A couple of comments regarding Eq. (30) are in order:

1. The (constant) density ρ_0 is proportional – in this case equal – to N, the number of rays per unit length. This makes sense: If you increase N, you increase the number of rays per unit length, hence the density ρ_0. If you decrease N, you decrease the density ρ_0.

2. The (constant) density ρ_0 is inversely proportional to Δa, the spacing between consecutive rays. This also makes sense. If you decrease Δa, you are increasing the number N of rays per unit length, i.e. the density ρ_0. If you increase Δa, you are decreasing the number N of rays per unit length, i.e., the density ρ_0.

These ideas will be important in the discussion that follows.

In a manner analogous to Eq. (30), we now define the (constant) lineal density, σ_n, of reflected rays the interval J_n as the number of rays per unit length which, in turn, is the reciprocal of the (constant) spacing, Δb_n, of the rays on J_n. From Eq. (29),

$$\sigma_n = \frac{1}{\Delta b_n} = \sin 2\theta_n\,\left[\frac{1}{\Delta a}\right] = \rho_0\,\sin 2\theta_n\,, \qquad n \geq 1\,. \tag{31}$$

Quick check: When $\theta_n = \dfrac{\pi}{4}$, the above equation implies that $\sigma_n = \rho_0$. As θ_n varies away from $\dfrac{\pi}{4}$, the density σ_n decreases. This looks good.

In fact, let us state this "quick check" result once again for emphasis:

> For all $\theta \in \left(0, \dfrac{\pi}{2}\right)$ except $\theta = \dfrac{\pi}{2}$, $\sigma_n < \rho_0$. This is a consequence of the fact that the length of interval J_n is **greater** than that of I_n except in the case $\theta = \dfrac{\pi}{2}$. Another way to see this is to use Eq. (22) to rewrite Eq. (31) as follows,
>
> $$\boxed{\sigma_n = \frac{\|J_n\|}{\|I_n\|}\,\rho_0\,.} \tag{32}$$

We can use Eq. (25) to express the relationship between σ_n and ρ_0 in terms of the slope m_n of the linear mirror piece supported on interval I_n:

$$\sigma_n = \left[\frac{2m_n}{m_n^2+1}\right]\rho_0\,, \qquad n \geq 1\,. \tag{33}$$

Graphical representations of densities are often helpful to understand the distributions of "things", in this case the intensities of incoming and reflected light rays. Firstly, the density function $\rho(x)$ of **incoming rays** over each interval, I_n, $n \geq 1$, on the x-axis is simply the constant function $\rho(x) = \rho_0$. Since the intervals I_n can overlap each other only at the endpoints, we can "paste" these individual graphs together to produce the graph of the net density function – the constant function $\rho(x) = \rho_0$ over the union of all intervals, I_n, as sketched in Figure 11 below. (The horizontal dotted lines have been added to emphasize the ends/endpoints of each individual component.)

In an effort – but a rather tiny one – to address the complications due to boundary points once again, we simply state that one can first construct the union of the graphs of individual constant functions $\rho = \rho_0$ over the **open intervals**, $I_n = (x_{n-1}, x_n)$ to produce the constant function $\rho(x) = \rho_0$ which is defined over all x except the boundary points x_n. One can then "fill up" this "graph with holes" by defining $\rho(x_n) = \rho_0$ to produce the constant function $\rho(x)$ defined over all x (or at least all x considered in this problem).

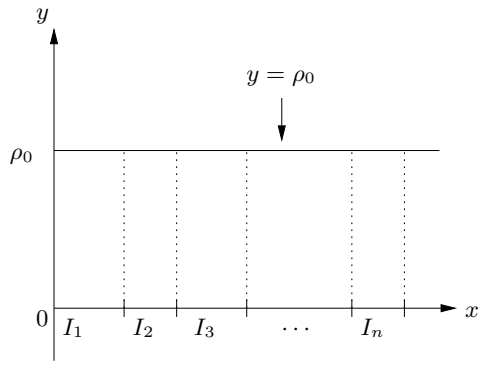

Figure 11: Plot of constant density function, $y = \rho_0$, for incoming rays over intervals I_n, $n \geq 1$.

We now turn our attention to the densities of the reflected rays on the y-axis. As discussed above, there is a (constant) density σ_n of reflected rays hitting each interval J_n, $n \geq 1$, on the y-axis as per Eq. (31) or (33). The graph of the portion of the density function $\sigma(y)$ of reflected rays over J_n will then be the constant function $\sigma(y) = \sigma_n$. The resulting graph of the net density function $\sigma(y)$ of reflected rays will have to involve a union of these constant functions over the interval. As discussed earlier, however, there is the additional complication that the intervals J_n could overlap with each other at more than simply boundary points. Such a situation is sketched in Figure 12 below. The natural question is, "How do we combine the graphs of (possibly different) constant densities which are supported on overlapping intervals?"

The answer to this question is easy for a point $y = y_1$ which lies in only one interval, say J_1. At that y, the density $\sigma(y_1)$ will simply be σ_1 since the only rays coming to it (or near it) are being reflected from the mirror which is located over the interval I_1, i.e., incoming rays which are located over the interval I_1.

But what about a point $y = y_2$ which lies in two intervals, say J_1 and J_2? This means that y_2 (more properly, a neighbourhood of y_2 is receiving reflected rays from two sources: (1) incoming rays located at interval I_1 and (2) incoming rays located at I_2. From our earlier discussion, source (1) produces reflected rays with density σ_1 which implies (from the definition of density) that there are σ_1 rays per unit length coming from source (1) and arriving in the vicinity of y_2. And source (2) produces reflected rays with density σ_2, meaning that there are σ_2 rays per unit length coming from source (2) and arriving in the vicinity of y_2. Of course, the result is that there is a net flux of $\sigma_1 + \sigma_2$ rays per unit length coming from both sources. In other words, *density functions are additive*: At any such y_2 which belongs to both J_1 and J_2, $\sigma(y_2) = \sigma_1 + \sigma_2$.

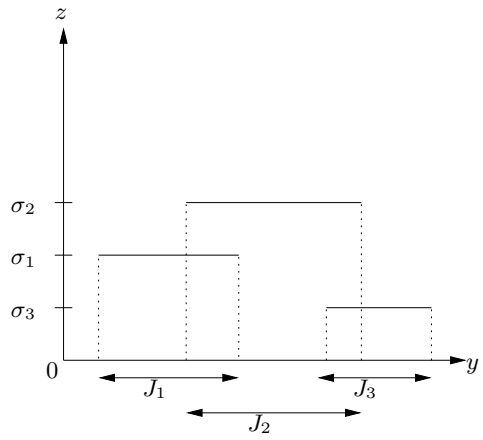

Figure 12: Plot of constant density functions, $z = \sigma_k(y)$, of reflected rays over overlapping intervals J_k, $k = 1, 2, 3$.

The generalization of this example should be clear: At each y, we add up the densities σ_k corresponding to all intervals J_k in which y lies. The net result is a kind of "sum" of the graphs as sketched in Figure 12. (Possible y_1 and y_2 values discussed in the previous paragraph have been identified in the figure.) The resulting density function $\sigma(y)$ will be a piecewise constant function – it is shown with thicker lines.

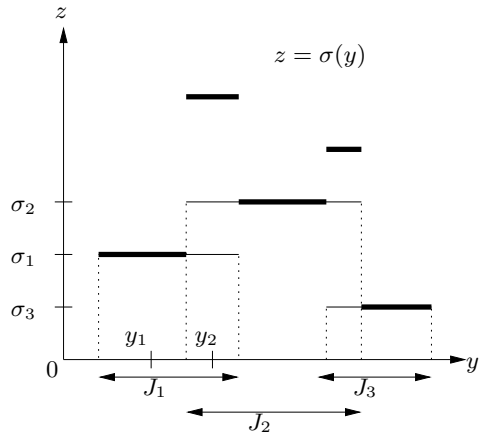

Figure 13: Plot of net density function, $z = \sigma(y)$, composed as a union of graphs of the constant density functions $z = \sigma_k$ defined over the overlapping intervals J_k, $k = 1, 2, 3$.

A return to the piecewise linear approximation of $f(x) = x^2$

In order to illustrate this fact, we show below once again the results presented in Table 1 of this report but slightly rearranged in order to present them as the endpoints $[x_{n-1}, x_n]$ of intervals I_n, $1 \leq n \leq 5$, (incoming rays) which are accompanied by the endpoints $[d_n, e_n]$ of the intervals J_n, $1 \leq n \leq 5$, (reflected rays) which were computed from the endpoints x_n of the J_n using Eqs. (13) and (14).

n	x(n-1)	x(n)	d(n)	e(n)
1	0.0000000000	0.3176872874	0.0000000000	0.5504626063
2	0.3176872874	0.5673059903	0.1398353622	0.3913193862
3	0.5673059903	0.7671940331	0.1558549160	0.3641226988
4	0.7671940331	0.9359675009	0.1604854457	0.3537567960
5	0.9359675009	1.0838643199	0.1624811061	0.3484556284

Perhaps the most remarkable observation to be made is that the intervals J_n not only overlap with each other but that they form a nested sequence, i.e.,

$$I_1 \supset I_2 \supset I_3 \supset I_4 \supset I_5 \,. \tag{34}$$

This can be explained, at least in part, by the concave upward nature of the function $f(x) = x^2$ which has been linearly interpolated to produce the above data. Recall that the individual linear "pieces" have the same length $b = \dfrac{1}{3}$. As n increases from 1, the "pieces" supported on the intervals I_n rotate counterclockwise. This implies that (1) the intervals I_n are getting shorter and (2) the intervals J_n are moving leftward.

The contents of the above table have been used to construct the piecewise constant density function $\sigma(y)$ for the mirror composed of the five "pieces" that comprise the piecewise linear interpolation of the function $f(x) = x^2$ shown in Figure 1. A plot of $\sigma(y)$ is shown in Figure 13. It can be compared with the "bin histogram" approximation for the same distribution shown in Figure 1.

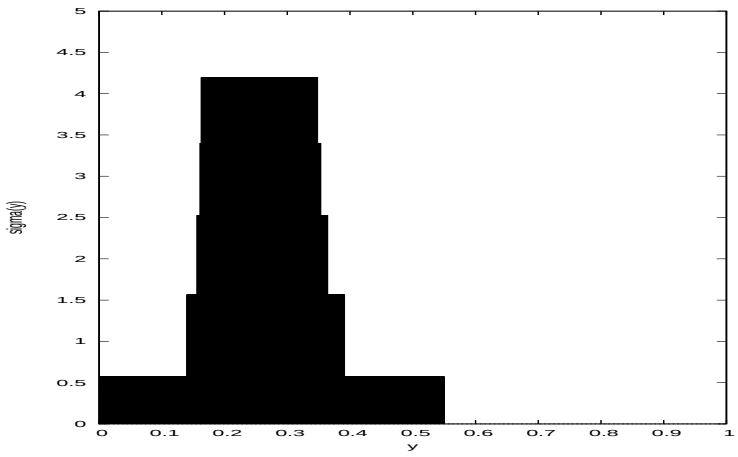

Figure 13: Plot of reflected ray density function $\sigma(y)$ produced by mirror surface defined by piecewise linear interpolation of $f(x) = x^2$ with five "pieces" of length $b = \dfrac{1}{3}$.